eXPRESS Polymer Letters Vol.12, No.3 (2018) 265–283
Available online at www.expresspolymlett.com
https://doi.org/10.3144/expresspolymlett.2018.24

sp^2 carbon allotropes in elastomer matrix: From master curves for the mechanical reinforcement to lightweight materials

M. Galimberti[1*], *G. Infortuna*[1], *S. Guerra*[1], *V. Barbera*[1], *S. Agnelli*[2], *S. Pandini*[2]

[1]Politecnico di Milano, Department of Chemistry, Materials and Chemical Engineering 'G. Natta', Via Mancinelli 7, 20131 Milano, Italy
[2]University of Brescia, Department of Mechanical and Industrial Engineering and INSTM UdR of Brescia, via Branze 38, 25123 Brescia, Italy

Received 29 August 2017; accepted in revised form 5 November 2017

Abstract. This work presents high surface area sp^2 carbon allotropes as important tools to design and prepare lightweight materials. Composites were prepared based on either carbon black (CB) or carbon nanotubes (CNT) or hybrid CB/CNT filler systems, with either poly(1,4-*cis*-isoprene) or poly(styrene-*co*-butadiene) as the polymer matrix. A correlation was established between the specific interfacial area (i.a.), i.e. the surface made available by the filler per unit volume of composite, and the initial modulus of the composite ($G'_{\gamma min}$), determined through dynamic mechanical shear tests. Experimental points could be fitted with a common line, a sort of master curve, up to about 30.2 and 9.8 mass% as CB and CNT content, respectively. The equation of such master curve allowed to correlate modulus and density of the composite. Thanks to the master curve, composites with the same modulus and lower density could be designed by substituting part of CB with lower amount of the carbon allotrope with larger surface area, CNT. This work establishes a quantitative correlation as a tool to design lightweight materials and paves the way for large scale application in polymer matrices of innovative sp^2 carbon allotropes.

Keywords: *rubber, carbon nanotubes, interfacial area, lightweight material, dynamic moduli*

1. Introduction

This work was performed in the frame of a research aimed at preparing lightweight high performance materials based on sp^2 carbon allotropes. Lightweight materials and design are at the edge of research in academic environment and in several industries, such as aerospace, automotive, wind power [1, 2] Reduction of CO_2 emission, particularly in automotive field, is the fundamental driver for the use of lightweight materials [3, 4]. Carbon materials, in particular fibres and nanomaterials [5] have been largely investigated and used for preparing lightweight materials [6–9]. This work was focused on polymer composites based on soft matrix and sp^2 carbon allotropes.

Soft materials such as polymer melts and elastomers achieve relevant mechanical properties thanks to the addition of the so called reinforcing fillers [10–13]. sp^2 carbon allotropes are known as efficient reinforcing fillers: carbon black (CB) [14, 15] has been used for over a century and, over the last decades, nanofillers such as carbon nanotubes (CNT) [16–18], graphene and graphene related materials (GRM) [19–21] have steadily increased their importance. CB is a nanostructured filler: it is made by primary nanometric particles, fused together to form micron-size aggregates. Nanofillers, such as CNT and GRM, can be separated into individual nanometric particles: they can establish large interfacial area with the polymer matrix and great impact on the material properties is thus expected.

Over the last years, an impressive number of new sp^2 carbon allotropes with nano dimensions have been

*Corresponding author, e-mail: maurizio.galimberti@polimi.it

prepared [22] and it is acknowledged that new allotropes are to be synthesized [23]. It was reported that major challenges arise aiming at 'combining low-dimensional forms into more complex 3D architectures' [23]. Intriguing research has thus to be performed on polymer nanocomposites based on sp^2 carbon allotropes and challenging objectives, indeed not yet achieved, are to identify common features and behavior for different families of allotropes and even to predict their behavior in a composite material.

It is nowadays clear that, particularly for large scale applications, nanofillers cannot replace CB. Indeed, increasing interest is on hybrid systems based on CB-CNT and CB-GRM [24], developed by partially substituting CB with nanometric carbon allotropes. In most studies, CB and carbon nanofillers have been separately investigated and only recently [25, 26] crystallinity, shape anisotropy, density, surface area and oil absorption of CNT, a nanosized graphite and CB have been compared.

Interestingly, synergistic effects on mechanical reinforcement, between CB and nanofillers, have been shown in both elastomeric [17, 24, 25, 27–30] and thermoplastic [31] matrices. Previous works by the authors highlighted that the mechanical reinforcement of an elastomer matrix promoted by hybrid fillers is not the result of the simple addition of reinforcing effects by each single filler [25, 30]. In fact, for a composite with a hybrid filler system composed by two fillers (filler A and filler B), the modulus of the hybrid filler composite, $G'_{hc}(\Phi_A, \Phi_B)$, was found to be larger than the one calculated as the sum of individual contributions by each single filler. This modulus increase was due to the interaction between the fillers and was expressed with an 'interaction term' ($\Delta G'_{int}$) [25, 32], through the Equation (1):

$$\Delta G'_{int}(\Phi_A, \Phi_B) = G'_{hc}(\Phi_A, \Phi_B) - G'_{matrix} - \\ -\left[G'_A(\Phi_A) - G'_{matrix}\right] - \left[G'_B(\Phi_B) - G'_{matrix}\right] \quad (1)$$

where the subscripts A and B refer to the two different fillers, Φ is the filler volume fraction, G'_{matrix} is the initial modulus of the neat matrix, $G'_A(\Phi_A)$ and $G'_B(\Phi_B)$ are the initial moduli of the composites with only filler A and with only filler B, respectively.

However, $\Delta G'_{int}(\Phi_A, \Phi_B)$ interaction term from Equation (1) provides only a phenomenological description of the interaction level. Moreover, to experimentally determine it, many experiments are required to assess its dependence on filler content: measurements of matrix modulus and of both single filler and hybrid filler composites have to be performed.

In order to rationalize the reinforcement data, a different approach based on the specific interfacial area was attempted. The interfacial area, i.a., is the surface made available by the filler per volume unit of composite. Correlation was found between i.a. and initial modulus of composites based on poly(1,4-*cis*-isoprene) and CB, CNT or CB/CNT hybrid filler system: a master curve was able to fit the experimental points [24, 25]. Recently, i.a. has been shown able to correlate also parameters of sulphur based crosslinking of natural rubber (NR), such as induction time (t_{s1}) and activation energy, in the presence of CNT, a high surface area nanosized graphite and CB: also in this case, master curves have been obtained [33].

If the master curves based on interfacial area had a general validity, they could be used as a tool for the rationalization of reinforcement, with many potential advantages. Master curves could allow to predict moduli of hybrid filler composites from the moduli of single filler composites, simply on the basis of the relative amount of fillers. Moreover, a compound with a given stiffness could be designed, calculating the amount of one or more fillers required to achieve the target modulus value. Furthermore, only few experiments would be needed to evaluate the master curve equation and predict the values required to determine the interaction term $\Delta G'_{int}(\Phi_A, \Phi_B)$, instead of the laborious approach based on many experiments [25].

This work is aimed at establishing a quantitative correlation between moduli at low strain amplitude of elastomer composites based on sp^2 carbon allotropes and a common feature of the carbon allotropes, both nanometric and nanostructured. Moreover, it is aimed at defining a quantitative tool to design lightweight elastomeric materials. Composites were prepared with either CNT or CB as the carbon allotropes, used as the only filler or as CNT/CB hybrid filler system. Characterization of carbon allotropes was performed by means of thermogravimetric analysis (TGA), wide angle X-ray diffraction (WAXD), Raman and Infrared (IR) spectroscopies, determination of surface area and pH and Boehm titration. Synthetic homo- and co-polymers were used as the matrices for the composites materials: poly(1,4-*cis*-isoprene) (IR) and poly(styrene-*co*-butadiene) (SBR). Composites were prepared via melt blending and were crosslinked with a peroxide, to avoid the effects of low molecular

mass substances traditionally used in sulphur based crosslinking, such as ZnO, stearic acid, sulphur and sulphenamide. The mechanical reinforcement was evaluated by dynamic moduli, and, in particular, modulus at minimum strain $G'_{\gamma_{min}}$ and $\Delta G'$ difference ($G'_{\gamma_{min}} - G'_{25\%}$) were considered. Objective of the research was to study the possibility to build master curves based not only on different carbon allotropes but also on different elastomers. Elastomers studied in the present work are traditionally used in tyre compounds. Lighter materials for tyre compounds can have a remarkable impact for the reduction of CO_2 emission.

2. Experimental part

2.1. Materials

Elastomers

Synthetic poly(1,4-*cis*-isoprene) (IR) was SKI3 (Nizhnekamskneftechim Export, Nizhnekamsk, Russia), with 70 Mooney Units (MU) as Mooney viscosity (M_L(1+4)100 °C). Synthetic poly(styrene-*co*-butadiene) (SBR) was from solution anionic polymerization: Nipol NS 522 (Zeon Corporation, Düsseldorf, Germany), with 39 mass% of bound styrene, 37.5 mass% of extension oil and 62 Mooney Units (MU) as Mooney viscosity (M_L(1+4)100 °C).

Peroxide

Luperox dicumyl-peroxide (Arkema Inc., Philadelphia, USA): 40% on $CaCO_3$ as the support.

Carbon allotropes

Carbon Black N326 (CB) was from Cabot Corporation (Billerica, USA), with 30 nm as mean diameter of spherical primary particles. DBP absorption number of 85 mL/100 g was measured and reported in [25]. Two types of Multiwall Carbon Nanotubes (CNT) were used: CNT(N) were NANOCYL® NC7000™ series from Nanocyl (Sambreville, Belgium), with carbon purity of 90% and average length of about 1.5 μm and CNT(B) were Baytubes® C150 P from Bayer Material Science AG (Leverkusen, Germany), with a chemical purity higher than 95 wt%, a length in the 1–10 μm range, a number of walls between 3 and 15 and outer and inner diameters of 10–16 and 4 nm respectively. Characterization of CNT(B) has been reported elsewhere [25]. In brief, CNT(B) has: BET surface area equal to 200 m^2/g, DBP absorption number of 316 mL/100 g and number of layers stacked in crystalline domain of about 10, measured by WAXRD analysis. In this work, characterization of CNT(N) (which are largely available on the commercial scale), is presented.

2.2. Composites

Formulations of composites based on IR

All the composites are based on 100 parts by weight of IR and 1.4 parts of dicumyl-peroxide. Various amounts of filler were added. Filler volumes% of composites based on IR as the polymer matrix are in Table 1. Three series of composites were prepared with various amounts of fillers: composites with only CB, with only CNT(B) and with hybrid filler systems, made by adding the same amount of CB and of CNT(B) in the composites.

Formulations of composites based on SBR

Also SBR based composites were prepared with 100 parts by weight of SBR, 1.4 parts of dicumyl-peroxide and various amounts of filler. The filler volumes% of composites based on SBR as the polymer matrix are in Table 2. Single filler composites, with only CB or only CNT(N), and hybrid filler composites were

Table 1. Filler volume % of composites based on IR, with CNT(B) and CB as the carbon allotropes[a]

Composites with only CNT(B)					
CNT(B)	1.2	2.4	4.7	9.0	12.9
Composites with only CB					
CB	1.2	2.4	4.7	9.0	12.9
Composites with the hybrid CNT(B)/CB filler system					
CNT(B) + CB	1.2	2.4	4.7	9.0	12.9
CNT(B)	0.6	1.2	2.4	4.5	6.5
CB	0.6	1.2	2.4	4.5	6.5

[a]further tests were performed, on the neat IR matrix and on composites with the following carbon fillers: with 1.7% CNT(B); with CB (volume %): 5.6, 16.6, 22.9, 26.3.

Table 2. Composites based on SBR, with CNT(N) and CB as the carbon allotropes[a]. CB volume %/CNT(N) volume % are indicated.

CB \ CNT(N)	0	2	4	6
0	0/0	0/2	0/4	0/6
5	5/0	5/2	5/4	5/6
10	10/0	10/2	10/4	10/6
15	15/0	15/2	15/4	15/6

[a]further tests were performed: with only CNT(N), with volume %: 0.5; 1.0; 1.4; 2.3; 2.8; 3.0; 3.4; 5.0; 8.0; 9.0; with only CB, with volume %: 7; 10; 13; 18; 24; 29, with hybrid filler system: 5 CB/1 CNT(N)

prepared. For the hybrid filler composites, systems were prepared with a given amount of CB (in the range from 0 to 15 as volume%), adding CNT(N) in a range from 0 to 6 of volume%.

Preparation

Composites, based on either IR or SBR, were prepared using a Brabender® type internal mixer (Brabender PL-2000 Plasti-Corder Torque Rheometer, Brabender GmbH & Co. KG, Duisburg, Germany), with 50 mL mixing chamber. The following procedure was adopted for the preparation of all the samples: 50 g of the polymer were introduced in the Brabender type internal mixer and masticated at 80 °C for 1 min with rotors rotating at 60 rpm. The filler was then added, mixing was performed for 4 min and the composite was then discharged at a temperature of about 90 °C. The composite, so prepared, was left to reach room temperature and was fed again to the Brabender® mixer kept at a temperature of about 50°C. Peroxide was added, mixing was performed for 3 minutes with rotors rotating at 60 rpm and composite was finally discharged. Composites were finally further homogeneized by passing them 5 times through a two roll mill operating at 50 °C, with the front roll rotating at 30 rpm and the back roll rotating at 38 rpm and 1 cm as the nip between the rolls.

Crosslinking

Reaction was performed at 170 °C for 10 min using a Monsanto oscillating disc rheometer (MDR 2000) (Alpha Technologies, Heilbron, Germany).

2.3. Characterization of carbon allotropes

Thermogravimetric analysis (TGA)

TGA tests were carried out under flowing N_2 (60 mL·min^{-1}) with a Mettler TGA SDTA/851 (Mettler-Toledo S.p.A., Novate Milanese, Milan, Italy) instrument according to the standard method ISO9924-1. Samples (10 mg) were heated from 30 to 800 °C at 10 °C·min^{-1}. After being maintained at 800 °C for 15 min, they were further heated up to 900 °C and kept for 30 min under flowing air (60 mL·min–1).

Wide angle X-ray diffraction (WAXD)

Wide-angle X-ray diffraction patterns were obtained in reflection, with an automatic Bruker D8 Advance diffractometer (Bruker Corporation, Billerica, Massachusetts, USA), with nickel filtered Cu–Kα radiation. Patterns were recorded in 10–100° as the 2θ range, being 2θ the peak diffraction angle. Distance between crystallographic planes was calculated from the Bragg's law. The $D_{hk\ell}$ correlation length, in the direction perpendicular to the *hkℓ* crystal graphitic planes, was determined applying the Scherrer equation (Equation (2)):

$$D_{hk\ell} = \frac{K\lambda}{\beta_{hk\ell}\cos\theta_{hk\ell}} \quad (2)$$

where K is the Scherrer constant, λ is the wavelength of the irradiating beam (1.5419 Å, Cu-Kα), $\beta_{hk\ell}$ is the width at half height, and $\theta_{hk\ell}$ is the diffraction angle. The instrumental broadening, b, was determined by obtaining a WAXD pattern of a standard silicon powder 325 mesh (99%), under the same experimental conditions. The width at half height, $\beta_{hk\ell} = (B_{hk\ell} - b)$ was corrected, for each observed reflection with $\beta_{hk\ell} < 1°$, by subtracting the instrumental broadening of the closest silicon reflection from the experimental width at half height, $B_{hk\ell}$.

Raman spectroscopy

Raman spectra of powder samples deposited on a glass slide were taken with a Horiba Jobin Yvon Labram HR800 dispersive Raman spectrometer equipped with Olympus BX41 microscope and a 50× objective (Horiba, Ltd., Kyoto, 601-8510 Japan). The excitation line at 632.8 nm of a He/Ne laser was kept at 0.5 mW in order to prevent samples degradation. The spectra were obtained as the average of four acquisitions (scan time: 30 s for each acquisition) with a spectral resolution of 2 cm^{-1}.

High-resolution transmission electron microscopy (HRTEM)

HRTEM investigations on CNT(N) sample taken from the water suspension sonicated for 10 min were carried out with a Philips CM 200 field emission gun microscope (FEI Company, Eindhoven, The Netherlands) operating at an accelerating voltage of 200 kV. Few drops of the water suspensions were deposited on 200 mesh carbon-coated copper grid and air dried for several hours before analysis. During acquisition of HRTEM images, the samples did not undergo structural transformation. Low beam current densities and short acquisition times were adopted. To estimate the number of stacked graphene layers and the dimensions of the stacks visible in HRTEM micrographs, the Gatan Digital Micrograph software was used.

Surface area
It was determined by using a BET apparatus according to ASTM D6556 method, with nitrogen as the gas.

Fourier transformed – infrared (FT-IR) spectroscopy
IR spectra were recorded in transmission mode (128 scan and 4 cm^{-1} resolution) in a diamond anvil cell (DAC) using a ThermoElectron FT-IR Continuum IR microscope (Thermo Fisher Scientific, Waltham, Massachusetts, USA).

Boehm titration
It was performed to quantitatively determine the content of oxygenated surface groups. In a typical experiment, 0.05 g of the carbon allotrope were dispersed in 50 mL of a 0.05 M NaOH solution and water removal was performed (see in the following). After stirring at room temperature for 24 h, the mixture was filtrated. Removal from the solution of the solid carbon allotrope is essential to avoid the reaction of deprotonated groups on carbon allotrope surface with HCl. A part of the solution (10 mL) was mixed with a water solution of HCl (0.05 N, 20 mL). The obtained mixture was titrated using a 0.05 M solution of NaOH.

CO_2 removal with N_2
CO_2 was removed from solution immediately before the titration: samples were poured in 40 mL glass vials equipped with a glass septum lids. N_2 was bubbled into the vial through a needle submerged in the solution. Bubbling rate was less than 1 mL/min. The time of degasification was 24 h. After degasification, the samples were transferred to a beaker that had been purged with the inert gas and covered with Parafilm®, to prevent absorption of atmospheric CO_2.

pH
pH of carbon allotropes was determined according to the standard ASTM D1512 method: in a 50 mL flask were poured carbon black (1.5 g) and H_2O (20 mL) in sequence. Two drops of acetone were also added to facilitate wettability of the carbon material. The resulting mixture was sonicated for 3 min in a 2 L sonication bath. After this period, pH was measured using an electronic pH meter.

2.4. Characterization of composites

Dynamic-mechanical measurements
Dynamic-mechanical measurements on crosslinked composites were performed with a Monsanto R.P.A. 2000 rheometer (Alpha technologies, Heilbron, Germany) in the torsion mode. For each sample, a first strain sweep (0.1–25% shear strain amplitude) was performed at 50 °C and 1 Hz, then the sample was kept in the instrument at the minimum strain amplitude (γ_{min} = 0.1%) for 10 min, to achieve fully equilibrated conditions. Finally, dynamic tests were performed at 50 °C at increasing strain amplitude (0.1–25% shear strain amplitude) with a frequency of 1 Hz.

3. Results and discussion

3.1. Characterization of sp^2 carbon allotropes

Characterization of CB and CNT was performed in order to highlight chemical, topological and structural differences among the nanostructured and the nanometric fillers. Characteristics of CNT(B) were reported in a previous paper [25] and are summarized in the experimental part. In the present work, comparative analysis was focused on CBN326 and CNT(N), selected as the representative of the high aspect ratio nanometric carbon allotrope.
Carbon purity and structure of CB and CNT(N) were first investigated. Thermogravimetric analysis was performed to assess carbon purity. Data are shown in Table 3.
Carbon content of CNT(N) and CB was found to be about 89 and 98% by mass, respectively. In both cases, the value of carbon content is in line with what reported in its technical data sheet (90%). Appreciable mass loss (about 6%) for CNT(N) below 800 °C (starting from 460 °C) could lead to hypothesize either the presence of organic substances or defects. The presence of a residue after the treatment at 800 °C is as well appreciable, about 5% by mass, and could be attributed to the catalyst used for CNT(N) preparation.
Structure of carbon allotropes was investigated by means of WAXD and Raman spectroscopies. WAXD patterns are in Figure 1 for CB (curve 1) and CNT(N) (curve 2).
Both samples of Figure 1 present broad 002 reflections. The out of plane correlation lengths were estimated, by applying the Scherrer equation, to be

Table 3. Mass losses of CNT(N) and CB, from TGA analysis

Sample	Mass loss [%]		
	0 °C < *T* < 800 °C	**> 800 °C**	**Residue**
CNT(N)	5.8	89.3	4.9
CB	1.3	98.0	0.7

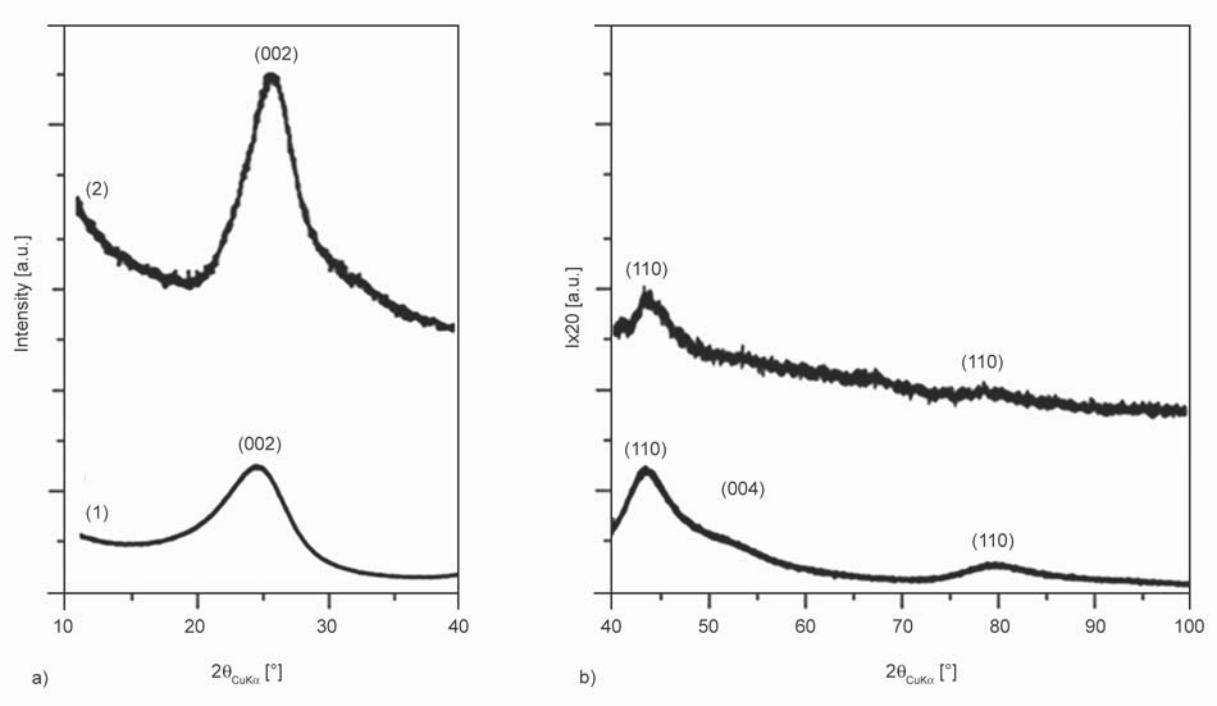

Figure 1. WAXD patterns of CB (1) and CNT(N) (2), a) from 10 to 40°, and b) from 40 to 100° as peak diffraction angle

about 1.9 and 3.0 nm for CB and CNT(N), which correspond to a number of layers stacked in crystalline domain of about 5 and 8, respectively. Both CB and CNT(N) present distances between the structural layers slightly larger than those of ordered graphite samples (d_{002} = 0.335 nm) [34]. Low intensity can be observed for the broad reflections characteristics of the order inside the graphitic planes. In both samples, 101 and 112 reflections are negligible. The absence of ($hk\ell$) reflections with $\ell \neq 0$, other than (002), is a clear indication of the structural disorder of CB and CNT(N). Indeed, it is widely acknowledged that CB has a turbostratic structure [35].

Raman spectra of CNT(N) and CB are reported in Figure 2.

The G peak is assigned to the E_{2g} Raman active mode of collective C=C stretching vibration of crystalline graphite (graphene), whereas the D peak appears when structural defects, such as holes, sp^3 or sp carbon atoms, dangling bonds, distortions from planarity, grafted functional groups or confinement (e.g. by edges) affect the graphitic layers [36–44]. Comparing the Raman features of CNT(N) and CB, several differences can be discerned. The number of observable modes in CB is clearly lower than that in CNT(N). In particular, the 2D [37] band can only be observed in CNT(N). Moreover, D and G peaks in CB spectrum are broader than in CNT(N) spectrum, indicating a higher degree of disorder. Accordingly, the I_D/I_G intensity ratios for CB and CNT(N) was

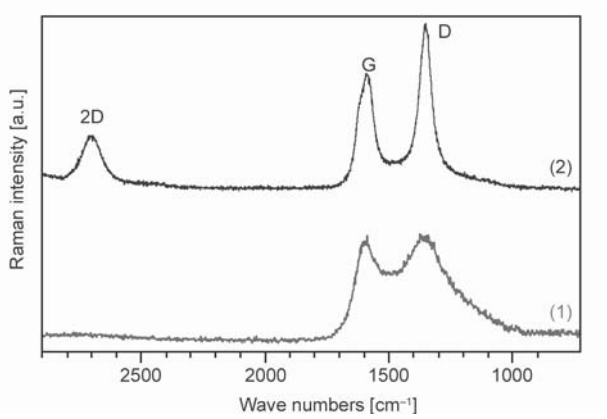

Figure 2. Raman spectra of CB (1) and CNT(N) (2)

estimated to be 1.7 and 1.3 respectively. Raman components between G and D peaks are due to disordered sp^3 carbon structures.

Morphological investigation of CNT(N) and CB samples was performed by means of HRTEM analysis at different magnifications. Micrographs are shown in Figure 3.

In Figure 3a, bundles of entangled CNT(N), lain on a grid, are clearly visible. Micrograph at high magnification in Figure 3b shows that the multiwalled CNT(N) skeleton is highly crystalline and regular. The inspection of such image allowed to estimate the average number of CNT(N) layers equal to 10, a value close to the one calculated from WAXD pattern.

Micrograph of CB at low magnification (Figure 3c) reveals carbon aggregates made by pseudo-spherical particles with an average size of about 30 nm.

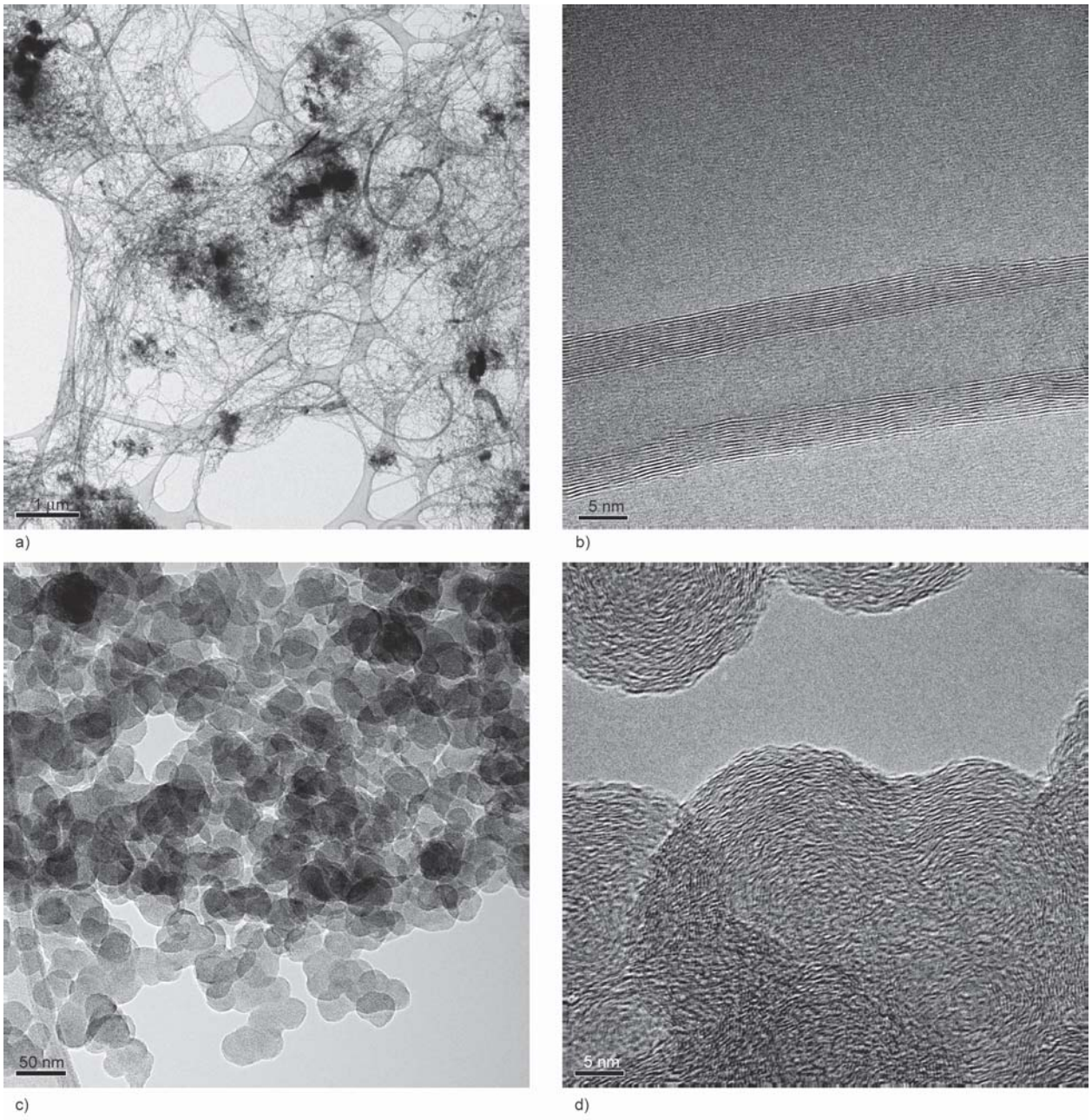

Figure 3. HRTEM micrographs of CNT(N) (a, b) and CB (c, d): at low (a, c) and higher (b, d) magnifications. In Figure a, the grid is visible

In Figure 3d it is evident the highly disordered graphitic structure.

As mentioned in the introduction, this work is aimed at identifying carbon fillers features suitable to establish common correlation with composites parameters and moves from results based on specific interfacial area as the correlation parameter. Hence, surface characteristics of CB and CNT(N) were investigated.

Surface area was determined through BET measurements. CB was found to have 77 m^2/g [25], a value close to those available in technical data sheet, 78 m^2/g, and in the literature, 75 m^2/g [45, 46]. Surface area was 200 m^2/g for CNT(B) and was 275 m^2/g for CNT(N), a value larger than the one reported in the literature, about 221 m^2/g [47], determined with 1-butene in place of nitrogen.

IR analysis was performed in order to identify the chemical nature of substances other than carbon (if any) present in CNT(N) and CB. In Figure 4, are shown IR spectra of CNT(N) (curve 1) and CB (curve 2): full spectra in the region 4000–700 cm^{-1} (Figure 4a) and the magnification in the region 1800–700 cm^{-1} after baseline correction (Figure 4b). IR spectra of CNT(N) and CB are characterized by the common strong feature at 1590 cm^{-1} assigned to E_{1u} IR active mode of the collective C=C stretching

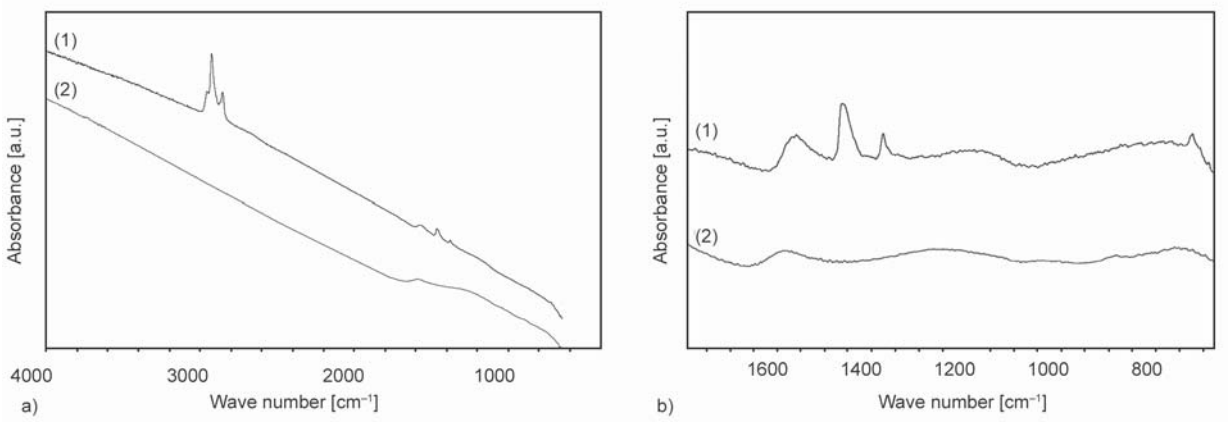

Figure 4. FTIR spectra of CNT(N) (1) and CB (2): full spectra in the region 4000–700 cm^{-1} (a) and magnification in the region 1800–700 cm^{-1} after baseline correction (b)

vibration of graphite and graphene materials [48]. The spectrum of CNT(N) clearly shows additional broad bands that can be assigned to vibrations of CH_2 and CH_3 groups located at 2952, 2921, and 1460 cm^{-1} and to vibration of alcohol groups OH, to bending of epoxy or ether groups at 1376, 1185 and 1100 cm^{-1}. These peaks support the indication of the mass loss at temperatures lower than 800 °C. Peaks characteristic of –COOR functionalities (acid and ester), which could be present in CNT(N) purified by means of acid treatment, could not be detected.

Content of oxygen functional groups on carbon filler surface was quantitatively evaluated using the Boehm titration method, which allows to determine groups such as carboxyls, lactones, lactols, epoxide and phenol [49, 50] The amounts of carbon surface functionalities were 1.3 mmol/g and 2 mmol/g for CB and CNT(N) respectively.

Boehm titration method provides information on the content of acidic oxygenated groups. Species such as ketones, aldehydes, ethers are not detected. However, these latter functional groups play a significant role in influencing the pH of the carbon allotrope. For this reason pH of carbon allotropes was also determined: for CB and CNT(N) was found to be 7.7 and 8.6 respectively.

Surface energy distribution was not measured in this work, but it has been reported in the literature for CNT(N) [47] and for a Carbon Black very close to the one used in this work, CBN347. It was determined by means of static 1-butene adsorption and it was reported that a good polymer filler interaction occurs on sites with energy of at least 27 kJ/mol. By performing a comparison with different types of CB, CNT(N) were found to have the lowest population of sites with at least this energy. In particular, CBN347 was commented to have appreciably larger surface activity than CNT(N). Explanation in the literature makes reference to the presence of different structures on CB surface: besides graphitic planes, also amorphous carbons, crystallite edges and slit shaped cavities [51].

The performed characterization allows to conclude that CB and CNT(N) have large carbon purity, of at least 90% by mass, disordered structure, dramatically different shape and surface area: CNT are nanosized tubes and CB is formed by sphere aggregates, with surface area larger than 200 m^2/g and of about 80 m^2/g, respectively. CNT are reported to have appreciably lower surface activity than CB [47] and in the present work were found to have larger amount of oxygenated groups and higher pH. Therefore, CB and CNT have bulk structure similarities and remarkable differences as to their shape and surface properties. The study aimed at finding a common rationalization of their behavior in elastomer composites is reported as follows.

3.2. Composites based on sp^2 carbon allotropes

Formulations of composites based on either IR or SBR as the polymer matrix and either CNT(N), CNT(B) or CB as the carbon allotropes, used as the only filler or as hybrid filler systems, are in Table 1 and in Table 2, respectively. Carbon allotropes content cover a very wide range of volume%, also to encompass the percolation thresholds of each filler and of the hybrid filler systems. In previous works by some of the authors, it was reported that the percolation threshold in IR [25] was at about 9 phr and at about 29 phr, for CNT(B) and CBN326 respectively. It was also shown [21, 28] that in the case of hybrid

filler systems, CB and the nanometric carbon allotropes are able to build a continuous hybrid system, with lowering of the percolation threshold. The carbon allotropes content covers as well a very wide range of specific interfacial area. Specific interfacial area (i.a.) is given by Equation (3):

$$\text{i.a.} = A_i \cdot \rho \cdot \phi \quad (3)$$

where A_i is the surface area (assumed to be equal to BET surface area), ρ is the filler density and ϕ is the filler volume fraction. The interfacial area is the surface made available by the filler per volume unit of composite. To emphasize this concept, in the text below, the measure unit of interfacial area is indicated as m^2/cm^3: m^2 indicate the surface made available by the filler and cm^3 indicate the volume unit of composite. In the case of composites based on IR, volume% indicated in the tables were achieved with only one filler or by combining CNT(B) and CB in equal amount. Results of composites already reported [25] were reproduced and reported along with other composites in order to achieve larger values of interfacial area, in particular with higher CB amount. In the case of composites based on SBR as the polymer matrix, a larger number of samples were prepared. Indeed, SBR is for the first time used for this type of investigation. Composites were prepared with either CNT(N) or CB as the only filler, in a wide range of volume%, and with hybrid filler systems, formed by adding to a given content of either CNT(N) or CB the other carbon allotrope, as shown in Table 2. Dispersion of CNT and CB and of the hybrid filler systems has been studied in previous works and reported in papers already published [25, 28]. Carbon fillers were observed to be homogeneously distributed and dispersed and to create continuous networks in the hybrid filler systems.

Mechanical behavior of crosslinked composites of Table 1 and Table 2 was studied by means of dynamic-mechanical tests performed in the shear mode (as described in the experimental part). Storage shear modulus G' was measured as a function of the strain, determining G' values up to 25% as strain amplitude ($G'_{25\%}$). G' values taken at the minimum shear strain amplitude (γ_{min} = 0.1% strain), $G'_{\gamma min}$, and $\Delta G'$ difference ($G'_{\gamma min} - G'_{25\%}$) were used to perform the analysis of reinforcement brought about by single or binary filler systems. Values of $G'_{\gamma min}$ and of $\Delta G'$ are reported Tables 4 and 5 for SBR and IR based composites, respectively.

Table 4. Filler volume %, specific surface area, $G'_{\gamma min}$ and $\Delta G'$ of SBR based composites

Composites with only CB				
CB [volume %]	**CNT [volume %]**	**i.a. [m^2/cm^3]**	**$G'_{\gamma min}$ [MPa]**	**$\Delta G'$ [MPa]**
0	0	0.0	0.43	0.04
5	0	6.9	0.59	0.07
7	0	9.7	0.60	0.09
7	0	9.7	0.63	0.13
10	0	13.9	0.74	0.18
10	0	13.9	0.85	0.22
13	0	18.0	0.88	0.27
15	0	20.8	1.06	0.36
18	0	24.9	1.40	0.60
24	0	33.3	2.00	1.12
29	0	40.2	3.17	2.09
Composites with only CNT(N)				
CB [volume %]	**CNT [volume %]**	**i.a. [m^2/cm^3]**	**$G'_{\gamma min}$ [MPa]**	**$\Delta G'$ [MPa]**
0	0.5	2.4	0.45	0.05
0	1.0	4.8	0.50	0.07
0	1.0	5.0	0.43	0.05
0	1.4	7.1	0.56	0.11
0	1.9	9.4	0.65	0.14
0	2.3	11.6	0.72	0.17
0	2.8	13.8	0.76	0.17
0	3.0	14.9	0.83	0.23
0	3.4	17.0	0.94	0.29
0	4.5	22.2	1.21	0.48
0	5.0	24.8	1.35	0.57
0	6.0	29.7	1.82	0.93
0	8.0	39.6	3.57	2.59
0	9.0	44.6	4.68	3.63
Composites with the hybrid CNT(N)/CB filler system				
CB [volume %]	**CNT [volume %]**	**i.a. [m^2/cm^3]**	**$G'_{\gamma min}$ [MPa]**	**$\Delta G'$ [MPa]**
5	1	11.9	0.59	0.11
5	2	16.8	0.91	0.24
5	4	26.7	1.83	0.88
5	6	36.6	2.82	1.73
10	2	23.8	1.53	0.72
10	4	33.7	2.98	1.98
10	6	43.6	5.60	4.27
15	2	30.7	2.79	1.76
15	4	40.6	4.61	3.42
15	6	50.5	9.49	7.86

Composites based on SBR and containing very similar amount of carbon allotropes were first investigated. In Figure 5a, are shown curves obtained by plotting G' values as a function of the shear strain amplitude for composites based on SBR with total volume% of carbon allotrope in the range between

Table 5. Filler volume %, specific surface area, $G'_{\gamma_{min}}$ and $\Delta G'$ of IR based composites

Composites with only CB				
CB [volume %]	**CNT [volume %]**	**i.a. [m²/cm³]**	**$G'_{\gamma_{min}}$ [MPa]**	**$\Delta G'$ [MPa]**
0.0	0	0.0	0.37	0.01
1.2	0	1.7	0.38	0.02
1.2	0	1.7	0.38	0.02
2.4	0	3.4	0.41	0.03
2.4	0	3.4	0.39	0.01
4.7	0	6.5	0.46	0.05
4.7	0	6.5	0.44	0.04
5.6	0	7.8	0.47	
9.0	0	12.5	0.58	0.09
9.0	0	12.5	0.54	0.06
12.9	0	17.9	0.72	0.17
16.6	0	22.9	0.99	0.37
22.9	0	31.8	1.81	1.00
26.3	0	36.5	3.07	2.09
Composites with only CNT(B)				
CB [volume %]	**CNT [volume %]**	**i.a. [m²/cm³]**	**$G'_{\gamma_{min}}$ [MPa]**	**$\Delta G'$ [MPa]**
0	1.2	4.4	0.43	0.04
0	1.7	6.1	0.48	0.10
0	2.4	8.7	0.53	0.13
0	2.4	8.7	0.51	0.08
0	4.7	17.0	0.73	0.19
0	9.0	32.5	1.26	0.54
0	12.9	46.6	2.29	1.41
Composites with the hybrid CNT(B)/CB filler system				
CB [volume %]	**CNT [volume %]**	**i.a. [m²/cm³]**	**$G'_{\gamma_{min}}$ [MPa]**	**$\Delta G'$ [MPa]**
0.6	0.6	3.0	0.41	0.03
1.2	1.2	6.0	0.46	0.04
2.4	2.4	11.8	0.59	0.09
2.4	2.4	11.8	0.56	0.14
4.5	4.5	22.5	0.88	0.25
6.5	6.5	32.3	1.50	0.78

0.09 and 0.1 (corresponding to 22 parts per 100 parts of polymer): composites with either CB or CNT(N) as the only carbon allotrope are compared with the composite based on the hybrid filler system.

Larger G' values were clearly obtained with CNT(N) as the reinforcing filler: $G'_{\gamma min}$ is more than five times higher than $G'_{\gamma min}$ of the composite based on CB. Storage moduli of the hybrid composites with almost the same amount of CB and CNT(N) are in between, closer to those of CB based composite. In Figure 5bare shown curves obtained by plotting G' vs shear strain for composites based on SBR and different contents of CNT(N): 1, 5, 9 as volume%. Larger nonlinearity of modulus can be observed for composites with larger amount of CNT(N).

It is acknowledged that a nanofiller such as CNT brings about large mechanical reinforcement of polymer melts and elastomers, definitely larger than the one obtained with CB. Results shown in Figure 5a, based on SBR matrix, confirm those already reported in IR as the matrix (see Figure 3 in ref. [25]). The graph in Figure 5 shows also a large reduction of modulus ($\Delta G'$) as the strain amplitude increases, that is a large nonlinearity of the modulus, for CNT(N) based composites. The modulus reduction is much larger for CNT(N) based composites than for CB based composite. This phenomenon, known as Payne effect [52], is mainly explained with models based on two main interpretations, which make reference either to filler-filler or to polymer-filler interactions: agglomeration–de-agglomeration process of the filler network above the filler percolation threshold [52–55] or polymer-filler bonding and debonding [56–64]. The reduction of storage modulus G' with the increase of the strain amplitude is linearly correlated with

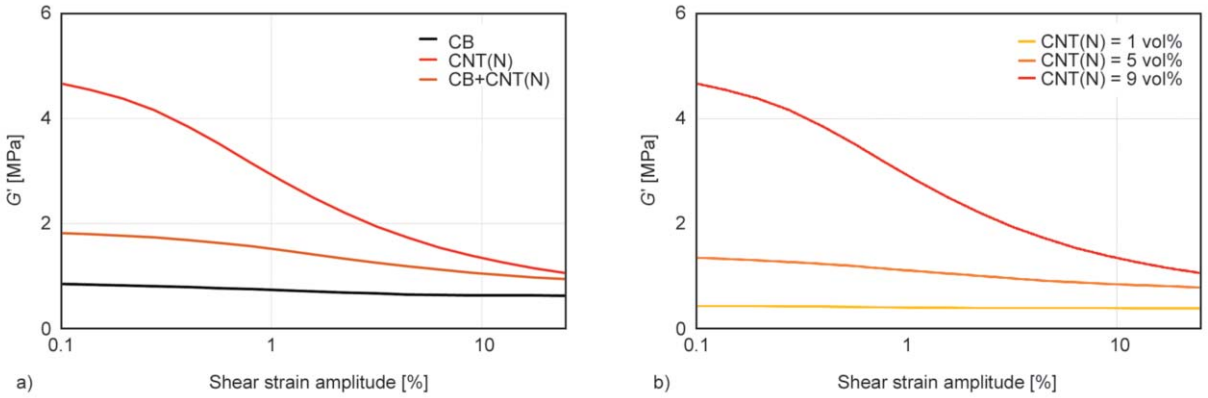

Figure 5. Storage shear modulus G' vs strain amplitude for SBR composites based on CNT(N), CB, CNT(N)/CB. (a) Composites with total volume %: 9 for CNT(N), 10 for CB and 4/5 for CNT(N)/CB; (b) composites with only CNT(N), volume %: 1, 5, 9.

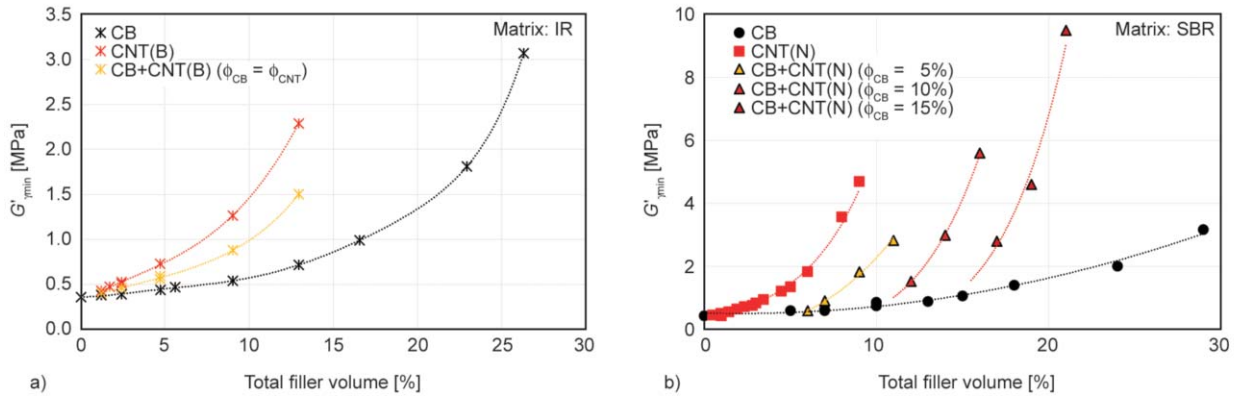

Figure 6. $G'_{\gamma min}$ vs total filler volume % for composites based on either IR (a) or SBR b) as the polymer matrix, with either CB or CNT or CB-CNT as the filler systems

the increase of the maximum value of loss modulus G''. Hence, for the same total filler volume%, polymer melts and elastomers based on CNT(N) undergo larger dissipation than composites based on CB.

The dependence of $G'_{\gamma min}$ on total filler volume% was then studied for all the composites of Table 1 and Table 2. Graphs in Figure 6 show such dependence for composites based on either IR (Figure 6a) or SBR (Figure 6b) as the polymer matrix, with either CB or CNT or the hybrid CB-CNT as the filler systems.

As commented above and shown in Table 1, for composites based on IR, hybrid filler systems were obtained with equal amounts of CNT(B) and CB: hence, only one curve is in Figure 6a for hybrid systems. In SBR, CNT(N) and CB were combined fixing the amount of CB (at 5, 10 and 15 as volume%) and adding various amounts of CNT(N) (see Table 2): three curves based on hybrid filler systems could be drawn in the graph of Figure 6b. The inspection of both figures reveals that, for the same total filler volume%, composites with CNT as the only filler have larger modulus than composites with CB as the only filler, whereas the curves due to hybrid filler systems lie in between.

The dependence, on the total filler volume%, of $\Delta G'(G'_{\gamma min} - G'_{25\%})$ is shown in Figure 7, for composites based on IR (Figure 7a) and on SBR (Figure 7b). In both graphs it can be clearly seen that composites containing CNT reveal higher nonlinearity of G' modulus with respect to composites with only CB as the filler.

As mentioned in the Introduction, objective of the present work was to establish a general correlation between mechanical reinforcement and feature(s) of sp^2 carbon allotropes. At the same level of filler amount and dispersion, the level of reinforcement promoted in a soft matrix depends on many factors, such as filler surface area, structure and surface activity. This work focuses the attention on filler surface area. In fact, the specific interfacial area, defined in Equation (3), was selected as the parameter for correlating $G'_{\gamma min}$ values for all the composites of Table 1 and Table 2. For the hybrid fillers, the total i.a. was calculated as the sum of the i.a. of each carbon filler in the composite, by applying Equation (4),

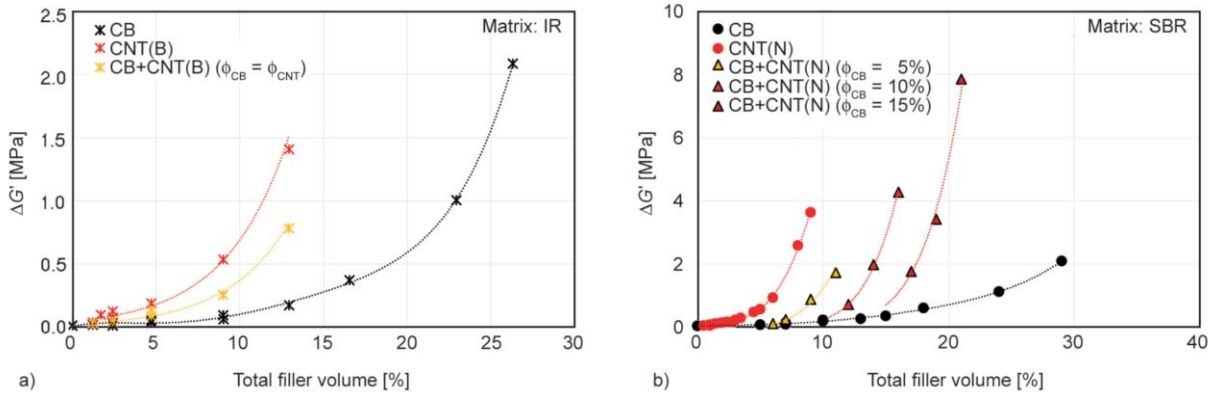

Figure 7. $\Delta G'$ vs total filler volume % for composites based on either IR (a) or SBR (b) as the polymer matrix, with either CB or CNT or CB-CNT as the filler systems

which is the extension of Equation (3) to the binary filler system:

$$\text{i.a.} = A_{iCB} \cdot \rho_{CB} \cdot \phi_{CB} + A_{iCNT} \cdot \rho_{CNT} \cdot \phi_{CNT} \quad (4)$$

As mentioned above, surface area is assumed equal to the BET value (77 m^2/g for CB, 200 m^2/g for CNT(B) and 275 m^2/g for CNT(N)) and $\rho_{CB} = \rho_{CNT} = 1.8$ g/cm^3 is the filler density.

Values of $G'_{\gamma min}$ shown in Figure 6 were normalized with respect to $G'_{\gamma min}$ of the matrix, and were plotted as a function of the interfacial area, calculated by applying Equation (3) and Equation (4).

The graph shown in Figure 8a was obtained. Magnification is shown in Figure 8b in the 0–25 (m^2/cm^3) interval of the interfacial area, with points fitted with an exponential curve.

It appears that points obtained for all the composites of Table 1 and Table 2 lie on the same exponential fitting curve (solid line in the graph of Figure 8b), a sort of master curve, up to a value of interfacial area of about 25 (m^2/cm^3), corresponding to CB and CNT(N) content of about 45 and 11.5 parts per hundred parts of polymer, respectively. Such contents are typical of many elastomer composites, reported in the scientific literature and also available at the commercial scale. This result is in line with the theory of reinforcement [10, 65], which says that modulus at low strains essentially depends on filler surface area. Moreover, it has been mentioned in the Introduction that the reinforcement changes with the specific interfacial area, for fillers with the same chemical nature [62]. However, it is definitely worth emphasizing that such a master curve holds for composites based on different elastomers and different carbon allotropes, nanometric and nanostructured, used as the only filler or in a hybrid filler system, with maximum carbon allotropes' contents well above their percolation threshold [25]. Different reasons could be at the origin of points' scattering for high values of interfacial area. Difficulties in mixing a nanofiller such as CNT could be taken into account. However, a more careful inspection of the graph seems also to suggest a way to handle such technical problem. In fact, it is interesting to observe that, in the scattered region, points of CNT filled systems based on IR lie below those based on SBR. It was reported in the literature the positive effect of aromatic rings, in polymers as well as in molecules used as surfactants, to promote CNT dispersion and to establish an intimate interaction between CNT and the polymer matrix. As an effect of well dispersed nanofiller particles, low electrical percolation thresholds were obtained for CNT in matrices made by polymers with aromatic repeating units: at about 0.5 as CNT volume% in an aromatic polyester based thermoplastic polyurethane [66] and at about 0.95 phr CNT in SBR [67], preparing the nanocomposites in both cases via solution blending. Stable dispersions of multiwalled CNT were prepared in chloroform, tetrahydrofuran and toluene by using methyl methacrylate copolymers with pyrene side groups randomly distributed along the chains [68]. Solubility in tetrahydrofuran was improved for single walled CNT thanks to styrene based copolymers with a pyrene block [69] and for multiwalled CNT thanks to pyrene functionalized polymers prepared with a pyrene functionalized RAFT agent [70].

This evidence seems to support the hypothesis that a better CNT dispersion is obtained when the matrix contains a polymer with aromatic rings. Even more interesting appear the larger $G'_{\gamma min}/G'_m$ values

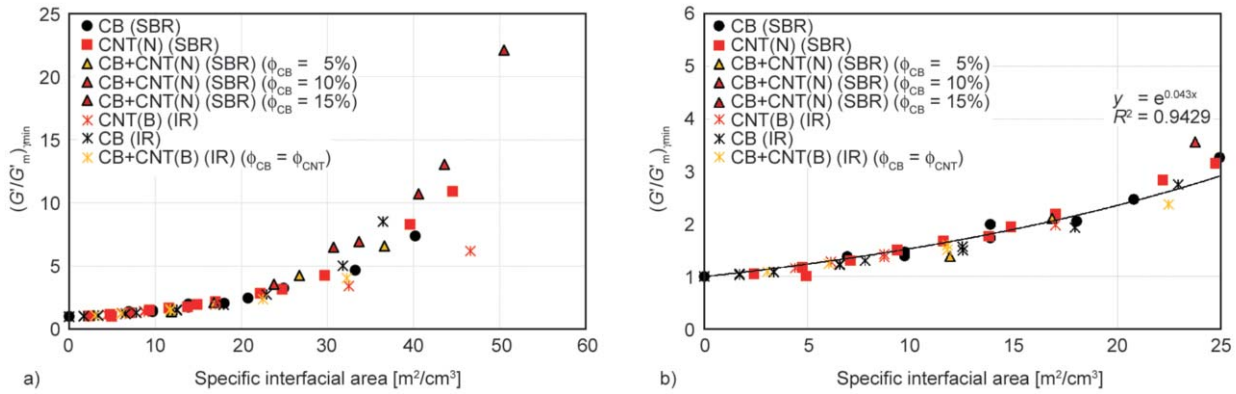

Figure 8. (a) $(G'/G'_m)_{\gamma min}$ vs specific interfacial area for composites of Table 1 and Table 2 (b) magnification of the 0–25 (m^2/cm^3) interval of the interfacial area with exponential fitting curve

obtained with hybrid CB/CNT systems. It is reported in the literature that CB helps CNT dispersion in a polymer matrix [71–74]. As already commented, synergistic effects on mechanical reinforcement have been reported for hybrid filler systems formed by nanometric and nano-structured carbon allotropes, such as CNT and CB [17, 24, 27–31].

Graphs in Figure 5a and Figure 6 and data in Tables 4 and 5 reveal the much larger reinforcing ability of CNT. Hence, besides considerations on cost and impact on human health, CNT appears to be an ideal filler for preparing elastomer composites with important mechanical properties.

However, CNT based composites show much more pronounced Payne effect than composites based on CB or on the hybrid CNT/CB system, as shown by the graphs of Figure 5b and in Figure 7. Such a remarkable Payne effect prevents the large scale application of CNT in composites designed for demanding dynamic-mechanical application, because of the large dissipation of energy which could be envisaged. It could be hypothesized that this behavior is intrinsically correlated with CNT. To investigate this aspect, values of $\Delta G'$ were plotted as a function of the interfacial area for all the composites of Table 1 and Table 2.

The graph shown in Figure 9 reveals that the same correlation observed in Figure 8 for G' values can be observed also for $\Delta G'$. The same values of $G'_{\gamma min}$ and of $\Delta G'$ can be thus obtained for elastomer composites with sp^2 carbon allotropes as the reinforcing fillers, when carbon fillers are used in such an amount to provide the same value of polymer filler interfacial area.

Correlation has been thus established between dynamic modulus of composites and specific interfacial area. It is even surprising that points were fitted with a common line, although a single filler feature was considered. Moreover, it could be also reasonably commented that BET surface area overestimates the surface area available to the polymer. As a matter of fact, as it is shown in Figure 8, fitting with an acceptable correlation coefficient occurs over a limited (though quite wide) range of carbon allotrope content and, the coefficient could be higher. Indeed, filler features such as surface activity, particles' anisometry and the actual availability of the filler surface to the interaction with polymer chains have been neglected. Improvement of the fitting with experimental data of mechanical reinforcement could be expected by considering also these features. In fact, in a previous work [25], it was shown a satisfactory correlation between specific surface area and composites' initial modulus for carbon nanotubes and carbon black but not for a high surface area nanosized graphite (HSAG). Comment was that, in the case of HSAG, the BET surface area measured by nitrogen absorption was not actually available to the polymer chain: graphene layers are prevailingly stacked in crystalline domains. To take into consideration this aspect, surface area could be determined with an organic molecule, such as cetylammonium bromide [10], in place of a gas. In this work correlation has been attempted between values of initial modulus and values of di-iso butyl phthalate (DBP) absorption of carbon allotropes, available for CB, CNT(B) and for the HSAG used in the cited work [25]. Measured DBP values were: 85 (CB), 316 (CNT(B)), 162 (HSAG) mL/100 g. DBP absorption values are typically used to estimate filler porosities available to the polymer chains. In the graph in Figure 10 reported below, initial modulus values of composites based on IR and SBR as the rubbers and CB, CNT(B) and HSAG as the fillers (data of HSAG based composites were taken from the cited work [25]) are plotted versus the effective volume fraction, calculated through the Medalia expression [75], reported below as Equation (5):

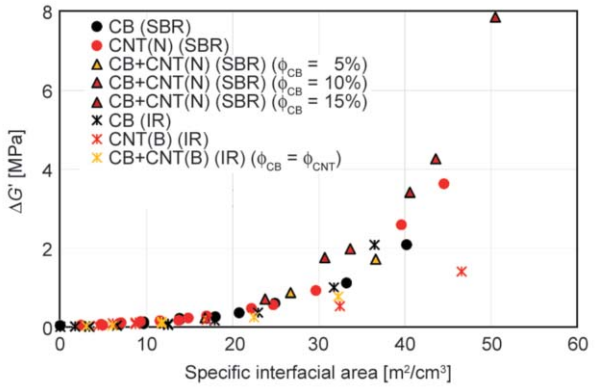

Figure 9. $\Delta G'$ vs specific interfacial area for composites of Table 1 and Table 2

$$\text{effective volume fraction} = \frac{\phi}{2}\left(1 + \frac{1 + 0.02139 \cdot DBP}{1.46}\right) \quad (5)$$

where DBP is the absorption value in mL/100 g. In case of hybrid filler systems, the total effective

volume fraction is calculated as the sum of the effective volume fraction calculated for each single filler.

It is indeed worth observing that points fit a common line, also for HSAG based composites and over a wider range of carbon allotrope content. It could be thus commented that a parameter such as the *DBP* absorption, which takes into account the actual interaction between the polymer and the filler, could be used to establish correlations with mechanical properties such as the moduli at low strain amplitude. Moreover, the comparative analysis of correlations based on surface area and DBP absorption allows to tell apart fillers, on the basis of their actual ability to interact with the polymer matrix. In case a new carbon allotrope would be used as filler, both charts of Figure 8 and Figure 10 would be useful to examine its reinforcing ability. As far as the effect of particles' anisometry is concerned, some of the authors have reently demonstrated [76] that anisometric carbon allotropes, such as CNT and HSAG, give rise to orthotropic and transversally isotropic mechanical properties. Moduli at low strains were found to be very similar in all directions inside the sheet plane, i.e. perpendicularly to the pressure applied during vulcanization, and appreciably different in orthogonal directions. Initial modulus values reported in the present work can indeed be compared, as they were determined inside the sheet plane.

Results reported so far allow to comment that the same values of $G'_{\gamma min}$ and of $\Delta G'$are obtained for elastomer composites with sp^2 carbon allotropes as the reinforcing fillers, when carbon fillers are used in such an amount to provide the same value of polymer filler interfacial area. Correlation has been thus

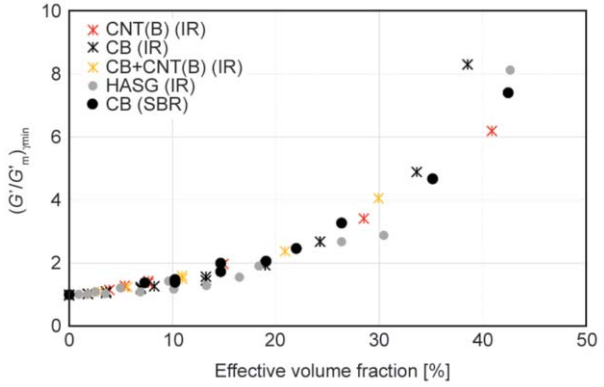

Figure 10. $(G'/G'_m)_{\gamma min}$ vs effective volume fraction (calculated through Equation (5), see text) for composites of Table 1 and Table 2 with CB, CNT(B) and HSAG (from [25]) as the carbon allotropes

established between dynamic modulus of composites and specific interfacial area. As reported in the Introduction, the aim of establishing this correlation was to design lightweight materials. In the following, it is shown an example of composite design, upon defining target values of dynamic modulus and density.

Target values of G' modulus were defined in a range covered by the master curve of Figure 7b. For such G' values, the corresponding interfacial area could be obtained by solving the equation of the master curve, Equation (6):

$$\frac{G'_{\gamma min}}{G'_m} = e^{0.043 i.a.} \tag{6}$$

The correlation between i.a. and the filler volume fraction of CB and CNT is given by Equation (4). CNT(N) were considered in this calculation.

For given values of filler volume fractions, the density of the composite (ρ_C) could be calculated by using Equation (7):

$$\rho_C = \rho_{CB} \cdot \phi_{CB} + \rho_{CNT} \cdot \phi_{CNT} + \\ + \rho_m \cdot (1 - \phi_{CB} - \phi_{CNT}) \tag{7}$$

Equation (7) is based on the rule of mixtures, under the assumption that the composites include only the elastomer matrix and the filler(s) (the presence of peroxide is thus neglected). Equation (7) provides a rough estimation of the density of the composite. It could be commented that a large part of highly-filled rubber compounds is bound rubber and bound rubber is expected to have a density higher than the matrix density. However, rubber density (also bound rubber) cannot be considered higher than the filler density. Moreover, density difference is expected to be not relevant for the calculations according to Equation (7). In the literature [77] it was reported that, in the case of NR, density value should be between that of amorphous and crystalline NR: these values range between 0.9 and 0.96. The variation of matrix density is below 6%, and this gives an uncertainty of the density of the composite even lower. The density of the SBR matrix, ρ_m, was estimated equal to 0.98 g/cm^3.

$G'_{\gamma min}$ interfacial area values of Equation (4) could be obtained by using different amounts of CNT(N) and CB, as single fillers or in hybrid filler systems.

To have lighter composites, larger amount of CNT(N) should be used. The ratio between the CNT(N) amount and the total filler amount, here defined as

$\phi_{CNT}/(\phi_{CB} + \phi_{CNT})$, ranges from 0, for composites based only on CB, to 1 for composites based only on CNT(N). Composite density was plotted as a function of $\phi_{CNT}/(\phi_{CB} + \phi_{CNT})$ for composites based on SBR with different $G'_{\gamma min}$ modulus, in a range from 0.43 to 1.56 MPa. Curves were obtained and are shown in the graph in Figure 11.

Composite density decreases as the CNT(N) relative content increases and, for a given modulus, achieves the minimum values when only CNT(N) is used as the filler. Reduction is larger when target modulus value is higher: for example, for the composite with 1.56 MPa as the target modulus, reduction of density is of about 11%.

Curves in Figure 8b and 11 and Equation (6) allow to design light weight material, through the following path. Target value of initial modulus can be defined, e.g. 1.37 MPa. This modulus can be achieved using only CB: the amount of CB required is 19.5 as volume% and 32.3 as mass%. It can be then defined target reduction of density. By using Equation (4) and taking into account that CB and CNT(N) have the same density, reduction of composite density form 1.14 to 1.07 g/cm^3 can be achieved by substituting 30% by mass of CB with the same amount of CNT(N). This composite would have 7.7 and 3.3 as volume% of CB and CNT(N), respectively. It must be pointed out that the partial substitution of CB with CNT(N) at the same i.a. does not alter the dissipative behaviour of the materials, since also the Payne effect follows a master curve with the i.a. (as shown in Figure 9).

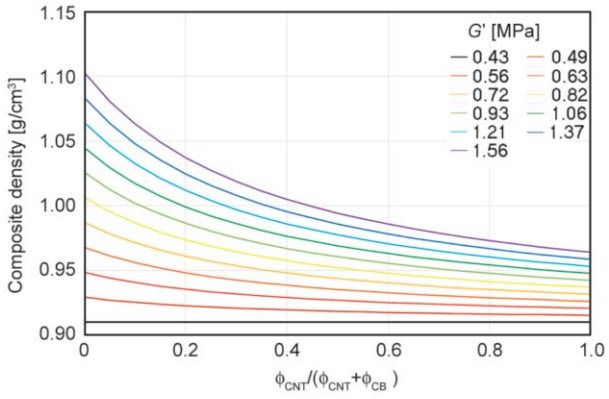

Figure 11. Composite density as a function of $\phi_{CNT}/(\phi_{CB} + \phi_{CNT})$ for composites based on SBR with $G'_{\gamma min}$ modulus in the range from 0.43 to 1.56 MPa

4. Conclusions

Results of this work are a contribution for using sp^2 carbon allotropes, particularly the ones with high surface area, for the preparation of lightweight materials. Modulus at low strain amplitude was determined by dynamic-mechanical measurements in the shear mode for composites based on either poly(1,4-*cis*-isoprene) or poly(styrene-*co*-butadiene) as the polymer matrix, with either carbon black or carbon nanotubes or hybrid filler systems. By plotting initial modulus as a function of the specific interfacial area, experimental points were fitted with a common curve, sort of master curve, up to a CB and CNT(N) content of about 30.2 and 9.8 as mass%. Common correlation with interfacial area was found also for $\Delta G'(G'_{\gamma min} - G'_{25\%})$, that is for the reduction of the initial modulus with the strain amplitude. This result demonstrates that large non linearity of the dynamic modulus typical of CNT based composites is not intrinsically correlated with CNT, but is simply the consequence of the surface area of the carbon allotrope.

The master curve of the initial modulus teaches that, by using sp^2 carbon allotropes with the same density, target modulus can be obtained by substituting CB with lower volume% of CNT, thus obtaining lighter composites. For instance, it was calculated a density reduction from 1.14 to 1.07 g/cm^3, for an SBR based composite with 1.37 MPa as the modulus, can be obtained by substituting 30% by mass of CB with CNT. In a nutshell, this work establishes for the first time a quantitative correlation as a tool to design nanofilled and hybrid filled elastomeric lightweight materials.

Acknowledgements

Authors gratefully acknowledge Prof. Chiara Castiglioni and Dr. Luigi Brambilla (Politecnico di Milano) for RAMAN and FT-IR analysis.

References

[1] Mayyas A., Qattawi A., Omar M., Shan D.: Design for sustainability in automotive industry: A comprehensive review. Renewable and Sustainable Energy Reviews, **16**, 1845–1862 (2012). https://doi.org/10.1016/j.rser.2012.01.012

[2] Kulkarni S., Dabeer P., Kale S., Sawant S. M.: Comprehensive evaluation of some innovative wind turbines. in 'ASME 2015 International Mechanical Engineering Congress and Exposition, Huston, USA' Vol 14, V014T06A006–V014T06A017 (2015). https://doi.org/10.1115/IMECE2015-53463

[3] Wenlong S., Xiaokai C., Lu W.: Analysis of energy saving and emission reduction of vehicles using light weight materials. Energy Procedia, **88**, 889–893 (2016). https://doi.org/10.1016/j.egypro.2016.06.106

[4] Goede M., Stehlin M., Rafflenbeul L., Kopp G., Beeh E.: Super light car – Lightweight construction thanks to a multi-material design and function integration. European Transport Research Review, **1**, 5–10 (2009). https://doi.org/10.1007/s12544-008-0001-2

[5] Coelho M. C., Torrão G., Emami N., Gracio J.: Nanotechnology in automotive industry: Research strategy and trends for the future – Small objects, big impacts. Journal of Nanoscience and Nanotechnology, **12**, 6621–6630 (2012). https://doi.org/10.1166/jnn.2012.4573

[6] Ozden S., Tsafack T., Owuor P. S., Li Y., Jalilov A. S., Vajtai R., Tiwary C. S., Lou J., Tour J. M., Mohite A. D., Ajayan P. M.: Chemically interconnected light-weight 3D-carbon nanotube solid network. Carbon, **119**, 142–149 (2017). https://doi.org/10.1016/j.carbon.2017.03.086

[7] Hemrick J. G., Lara-Curzio E., Loveland E. R., Sharp K. W., Schartow R.: Woven graphite fiber structures for use in ultra-light weight heat exchangers. Carbon, **49**, 4820–4829 (2011). https://doi.org/10.1016/j.carbon.2011.06.094

[8] Sundaram R. M., Windle A. H.: One-step purification of direct-spun CNT fibers by post-production sonication. Materials and Design, **126**, 85–90 (2017). https://doi.org/10.1016/j.matdes.2017.04.011

[9] Huda Z., Edi P.: Materials selection in design of structures and engines of supersonic aircrafts: A review. Materials and Design, **469**, 552–560 (2013). https://doi.org/10.1016/j.matdes.2012.10.001

[10] Donnet J. B., Custodero E.: Reinforcement of elastomers by particulate fillers. in 'The science and technology of rubber' (eds: Mark J. E., Erman B., Eirich F. R.), Academic Press, San Diego, 367–400 (2005).

[11] Hamed G. R.: Rubber reinforcement and its classification. Rubber Chemistry and Technology, **80**, 533–544 (2007). https://doi.org/10.5254/1.3548178

[12] Bokobza L.: The reinforcement of elastomeric networks by fillers. Macromolecular Materials and Engineering, **289**, 607–621 (2004). https://doi.org/10.1002/mame.200400034

[13] Heinrich G., Klüppel M., Vilgis T. A.: Reinforcement of elastomers. Current Opinion in Solid State and Materials Science, **6**, 195–203 (2002). https://doi.org/10.1016/S1359-0286(02)00030-X

[14] Gerspacher M., Wampler W.: Fillers: Carbon black. in 'Basic elastomer technology' (eds.: Baranwal K. C., Stephens H. L.), Rubber Division of the ACS, New York, 57–81 (2001).

[15] Wang M-J., Gray C. A., Reznek S. A., Mahmud K., Kutsovsky Y.: Carbon black. in 'Kirk-Othmer encyclopedia of chemical technology' (ed.: Seidel A.) Wiley, New York, 761–803 (2004). https://doi.org/10.1002/0471238961.0301180204011414.a01.pub2

[16] Maiti M., Bhattacharya M., Bhowmick A. K.: Elastomer nanocomposites. Rubber Chemistry and Technology, **81**, 384–469 (2008). https://doi.org/10.5254/1.3548215

[17] Galimberti M., Cipolletti V., Musto S., Cioppa S., Peli G., Mauro M., Guerra G., Agnelli S., Riccò T., Kumar V.: Recent advancements in rubber nanocomposites. Rubber Chemistry and Technology, **87**, 417–442 (2014). https://doi.org/10.5254/rct.14.86919

[18] Bokobza L.: Multiwall carbon nanotube elastomeric composites: A review. Polymer, **48**, 4907–4920 (2007). https://doi.org/10.1016/j.polymer.2007.06.046

[19] Bhattacharya M., Maiti M., Bhowmick A. K.: Tailoring properties of styrene butadiene rubber nanocomposite by various nanofillers and their dispersion. Polymer Engineering and Science, **49**, 81–98 (2009). https://doi.org/10.1002/pen.21224

[20] Al-solamy F. R., Al-Ghamdi A. A., Mahmoud W. E.: Piezoresistive behavior of graphite nanoplatelets based rubber nanocomposites. Polymers for Advanced Technologies, **23**, 478–482 (2012). https://doi.org/10.1002/pat.1902

[21] Galimberti M., Kumar V., Coombs M., Cipolletti V., Agnelli S., Pandini S., Conzatti L.: Filler networking of a nanographite with a high shape anisotropy and synergism with carbon black in poly(1,4-*cis*-isoprene)–based nanocomposites. Rubber Chemistry and Technology, **87**, 197–218 (2014). https://doi.org/10.5254/rct.13.87903

[22] Terrones M., Botello-Méndez A. R., Campos-Delgado J., López-Urías F., Vega-Cantú Y. I., Rodríguez-Macías F. J., Elías A. L., Muñoz-Sandoval E., Cano-Márquez A. G., Charlier J-C., Terrones H.: Graphene and graphite nanoribbons: Morphology, properties, synthesis, defects and applications. Nano Today, **5**, 351–372 (2010). https://doi.org/10.1016/j.nantod.2010.06.010

[23] Zhang J., Terrones M., Park C. R., Mukherjee R., Monthioux M., Koratkar N., Kim Y. S., Hurt R., Frackowiak E., Enoki T., Chen Y., Chen Y., Bianco A.: Carbon science in 2016: Status, challenges and perspectives. Carbon, **98**, 708–732 (2016). https://doi.org/10.1016/j.carbon.2015.11.060

[24] Galimberti M., Agnelli S., Cipolletti V.: Hybrid filler systems in rubber nanocomposites. in 'Progress in Rubber Nanocomposites' (eds: Thomas S., Maria H. J.) Woodhead, Elsevier, 349–414 (2017). https://doi.org/10.1016/B978-0-08-100409-8.00011-5

[25] Agnelli S., Cipolletti V., Musto S., Coombs M., Conzatti L., Pandini S., Riccò T., Galimberti M.: Interactive effects between carbon allotrope fillers on the mechanical reinforcement of polyisoprene based nanocomposites. Express Polymer Letters, **8**, 436–449 (2014). https://doi.org/10.3144/expresspolymlett.2014.47

[26] Mauro M., Cipolletti V., Galimberti M., Longo P., Guerra G.: Chemically reduced graphite oxide with improved shape anisotropy. The Journal of Physical Chemistry C, **116**, 24809–24813 (2012). https://doi.org/10.1021/jp307112k

[27] Szeluga U., Kumanek B., Trzebicka B.: Synergy in hybrid polymer/nanocarbon composites. A review. Composites Part A: Applied Science and Manufacturing, **73**, 204–231 (2015). https://doi.org/10.1016/j.compositesa.2015.02.021

[28] Galimberti M., Coombs M., Riccio P., Riccò T., Passera S., Pandini S., Conzatti L., Ravasio A., Tritto I.: The role of CNTs in promoting hybrid filler networking and synergism with carbon black in the mechanical behavior of filled polyisoprene. Macromolecular Materials and Engineering, **298**, 241–251 (2013). https://doi.org/10.1002/mame.201200075

[29] Dong B., Liu C., Lu Y., Wu Y.: Synergistic effects of carbon nanotubes and carbon black on the fracture and fatigue resistance of natural rubber composites. Journal of Applied Polymer Science, **132**, 42075–42082 (2015). https://doi.org/10.1002/app.42075

[30] Galimberti M., Cipolletti V., Coombs M., Riccò T., Agnelli S., Pandini S.: The role of nanofillers in promoting hybrid filler networking and synergism with carbon black in a hydrocarbon rubber. Kautschuk Gummi Kunstoffe, **66**, 31–36 (2013).

[31] Bhowmick A. K., Bhattacharya M., Mitra S.: Exfoliation of nanolayer assemblies for improved natural rubber properties: Methods and theory. Journal of Elastomers and Plastics, **42**, 517–537 (2010). https://doi.org/10.1177/0095244310383752

[32] Sternstein S. S., Ramorino G., Jang B., Zhu A-J.: Reinforcement and nonlinear viscoelasticity of polymer melts containing mixtures of nanofillers. Rubber Chemistry and Technology, **78**, 258–270 (2005). https://doi.org/10.5254/1.3547882

[33] Musto S., Barbera V., Cipolletti V., Citterio A., Galimberti M.: Master curves for the sulphur assisted crosslinking reaction of natural rubber in the presence of nano-and nano-structured sp^2 carbon allotropes. Express Polymer Letters, **11**, 435–448 (2017). https://doi.org/10.3144/expresspolymlett.2017.42

[34] Fujimoto H.: Theoretical X-ray scattering intensity of carbons with turbostratic stacking and AB stacking structures. Carbon, **41**, 1585–1592 (2003). https://doi.org/10.1016/S0008-6223(03)00116-7

[35] Li Z. Q., Lu C. J., Xia Z. P., Zhou Y., Luo Z.: X-ray diffraction patterns of graphite and turbostratic carbon. Carbon, **45**, 1686–1695 (2007). https://doi.org/10.1016/j.carbon.2007.03.038

[36] Ferrari A. C.: Raman spectroscopy of graphene and graphite: Disorder, electron–phonon coupling, doping and nonadiabatic effects. Solid State Communications, **143**, 47–57 (2007). https://doi.org/10.1016/j.ssc.2007.03.052

[37] Ferrari A. C., Meyer J. C., Scardaci V., Casiraghi C., Lazzeri M., Mauri F., Piscanec S., Jiang D., Novoselov K. S., Roth S., Geim A. K.: Raman spectrum of graphene and graphene layers. Physical Review Letters, **97**, 187401/1–187401/4 (2006). https://doi.org/10.1103/PhysRevLett.97.187401

[38] Reich S., Thomsen C.: Raman spectroscopy of graphite. Philosophical Transactions of the Royal Society of London A: Mathematical, Physical and Engineering Sciences, **362**, 2271–2288 (2004). https://doi.org/10.1098/rsta.2004.1454

[39] Pimenta M. A., Dresselhaus G., Dresselhaus M. S., Cançado L. G., Jorio A., Saito R.: Studying disorder in graphite-based systems by Raman spectroscopy. Physical Chemistry Chemical Physics, **9**, 1276–1290 (2007). https://doi.org/10.1039/b613962k

[40] Castiglioni C., Tommasini M., Zerbi G.: Raman spectroscopy of polyconjugated molecules and materials: confinement effect in one and two dimensions. Philosophical Transactions of the Royal Society A: Mathematical, Physical and Engineering Sciences, **362**, 2425–2459 (2004). https://doi.org/10.1098/rsta.2004.1448

[41] Graf D., Molitor F., Ensslin K., Stampfer C., Jungen A., Hierold C., Wirtz L.: Spatially resolved raman spectroscopy of single- and few-layer graphene. Nano letters, **7**, 238–242 (2007). https://doi.org/10.1021/nl061702a

[42] Casiraghi C., Hartschuh A., Qian H., Piscanec S., Georgi C., Fasoli A., Novoselov K. S., Basko D. M., Ferrari A. C.: Raman spectroscopy of graphene edges. Nano letters, **9**, 1433–1441 (2009). https://doi.org/10.1021/nl8032697

[43] Radovic L. R., Bockrath B.: On the chemical nature of graphene edges: Origin of stability and potential for magnetism in carbon materials. Journal of the American Chemical Society, **127**, 5917–5927 (2005). https://doi.org/10.1021/ja050124h

[44] Casiraghi C., Pisana S., Novoselov K. S., Geim A. K., Ferrari A. C.: Raman fingerprint of charged impurities in graphene. Applied Physics Letters, **91**, 233108–233114 (2007). https://doi.org/10.1063/1.2818692

[45] Kleemann W., Weber K.: Formeln und Tabellen für die Elastomerverarbeitung. Dr. Gupta Verlag, Düsseldorf (1994).

[46] Donnet J. B.: Carbon black: Science and technology. CRC Press, New York (1993).

[47] Dilman T., Jain A., Ludwig M., Giese U., Hasse A., Schwaiger B., Linster T., Marsat J. N.: Innovative polymer-filler systems with optimized damping and energy dissipation for the application in truck tires. in 'Proceedings of 11th Fall Rubber Colloquium, Hannover, Germany', p.8 (2014).

[48] Kim U. J., Liu X. M., Furtado C. A., Chen G., Saito R., Jiang J., Eklund P. C.: Infrared-active vibrational modes of single-walled carbon nanotubes. Physical Review Letters, **95**, 157402/1–157402/4 (2005). https://doi.org/10.1103/PhysRevLett.95.157402

[49] Boehm H. P.: Some aspects of the surface chemistry of carbon blacks and other carbons. Carbon, **32**, 759–769 (1994). https://doi.org/10.1016/0008-6223(94)90031-0

[50] Wepasnick K. A., Smith B. A., Bitter J. L. Fairbrother D. H.: Chemical and structural characterization of carbon nanotube surfaces. Analytical and Bioanalytical Chemistry, **396**, 1003–1014 (2010). https://doi.org/10.1007/s00216-009-3332-5

[51] Schröder A., Klüppel M., Schuster R. H.: Characterisation of surface activity of carbon black and its relation to polymer-filler interaction. Macromolecular Materials and Engineering, **292**, 885–916 (2007). https://doi.org/10.1002/mame.200700032

[52] Payne A. R., Whittaker R. E.: Low strain dynamic properties of filled rubbers. Rubber Chemistry and Technology, **44**, 440–478 (1971). https://doi.org/10.5254/1.3547375

[53] Robertson C. G., Roland C. M.: Glass transition and interfacial segmental dynamics in polymer-particle composites. Rubber Chemistry and Technology, **81**, 506–522 (2008). https://doi.org/10.5254/1.3548217

[54] Bohm G. A., Tomaszewski W., Cole W., Hogan T.: Furthering the understanding of the non linear response of filler reinforced elastomers. Polymer, **51**, 2057–2068 (2010). https://doi.org/10.1016/j.polymer.2010.01.047

[55] Heinrich G., Klüppel M.: Recent advances in the theory of filler networking in elastomers. in 'Filled elastomers drug delivery systems' (eds.: Abe A., Albertsson A-C., Coates G. W., Genzer J., Kobayashi S., Lee K-S., Leibler L., Long T. E., Möller M., Okay O., Percec V., Tang B. Z., Terentjev E. M., Theato P., Vicent M. J., Voit B., Wiesner U., Zhang X.) Volume 160, Springer, Berlin, 1–44 (2002). https://doi.org/10.1007/3-540-45362-8_1

[56] Maier P. G., Goritz D.: Molecular interpretation of the Payne effect. Kautschuk Gummi Kunststoffe, **49**, 18–21 (1996).

[57] Chazeau L., Brown J. D., Yanyo L. C., Sternstein S. S.: Modulus recovery kinetics and other insights into the Payne effect for filled elastomers. Polymer Composites, **21**, 202–222 (2000). https://doi.org/10.1002/pc.10178

[58] Sternstein S. S., Zhu A-J.: Reinforcement mechanism of nanofilled polymer melts as elucidated by nonlinear viscoelastic behavior. Macromolecules, **35**, 7262–7273 (2002). https://doi.org/10.1021/ma020482u

[59] Montes H., Lequeux F., Berriot J.: Influence of the glass transition temperature gradient on the nonlinear viscoelastic behavior in reinforced elastomers. Macromolecules, **36**, 8107–8118 (2003). https://doi.org/10.1021/ma0344590

[60] Zhu Z., Thompson T., Wang S-Q., von Meerwall E. D., Halasa A.: Investigating linear and nonlinear viscoelastic behavior using model silica-particle-filled polybutadiene. Macromolecules, **38**, 8816–8824 (2005). https://doi.org/10.1021/ma050922s

[61] Kalfus J., Jancar J.: Elastic response of nanocomposite poly(vinylacetate)-hydroxyapatite with varying particle shape. Polymer Composites, **28**, 365–371 (2007). https://doi.org/10.1002/pc.20273

[62] Jancar J., Douglas J. F., Starr F. W., Kumar S. K., Cassagnau P., Lesser A. J., Buehler M. J.: Current issues in research on structure–property relationships in polymer nanocomposites. Polymer, **51**, 3321–3343 (2010). https://doi.org/10.1016/j.polymer.2010.04.074

[63] Funt J. M.: Dynamic testing and reinforcement of rubber. Rubber Chemistry and Technology, **61**, 842–865 (1988). https://doi.org/10.5254/1.3536222

[64] Gauthier C., Reynaud E., Vassoille R., Ladouce-Stelandre L.: Analysis of the non-linear viscoelastic behaviour of silica filled styrene butadiene rubber. Polymer, **45**, 2761–2771 (2004). https://doi.org/10.1016/j.polymer.2003.12.081

[65] Medalia A. I.: Effect of carbon black on dynamic properties of rubber vulcanizates. Rubber Chemistry and Technology, **51**, 437–523 (1978). https://doi.org/10.5254/1.3535748

[66] Koerner H., Liu W., Alexander M., Mirau P., Dowty H., Vaia R. A.: Deformation–morphology correlations in electrically conductive carbon nanotube–thermoplastic polyurethane nanocomposites. Polymer, **46**, 4405–4420 (2005). https://doi.org/10.1016/j.polymer.2005.02.025

[67] Tsuchiya K., Sakai A., Nagaoka T., Uchida K., Futukawa T., Yajima H.: High electrical performance of carbon nanotubes/rubber composites with low percolation threshold prepared with a rotation–revolution mixing technique. Composites Science and Technology, **71**, 1098–1104 (2011). https://doi.org/10.1016/j.compscitech.2011.03.015

[68] Lou X., Daussin R., Cuenot S., Duwez A. S., Pagnoulle C., Detrembleur C., Bailly C., Jérôme R.: Synthesis of pyrene-containing polymers and noncovalent sidewall functionalization of multiwalled carbon nanotubes. Chemistry of Materials, **16**, 4005–4011 (2004). https://doi.org/10.1021/cm0492585

[69] Bahun G. J., Wang C., Adronov A.: Solubilizing single-walled carbon nanotubes with pyrene-functionalized block copolymers. Journal of Polymer Science Part A: Polymer Chemistry, **44**, 1941–1951 (2006). https://doi.org/10.1002/pola.21308

[70] Meuer S., Braun L., Schilling T., Zentel R.: α-pyrene polymer functionalized multiwalled carbon nanotubes: Solubility, stability and depletion phenomena. Polymer, **50**, 154–160 (2009). https://doi.org/10.1016/j.polymer.2008.10.039

[71] Junkong P., Kueseng P., Wirasate S., Huynh C., Rattanasom N.: Cut growth and abrasion behaviour, and morphology of natural rubber filled with MWCNT and MWCNT/carbon black. Polymer Testing, **41**, 172–183 (2015). https://doi.org/10.1016/j.polymertesting.2014.11.009

[72] Thaptong P., Sirisinha C., Thepsuwan U., Sae-Oui P.: Properties of natural rubber reinforced by carbon black-based hybrid fillers. Polymer-Plastics Technology and Engineering, **53**, 818–823 (2014). https://doi.org/10.1080/03602559.2014.886047

[73] Bokobza L.: Mechanical, electrical and spectroscopic investigations of carbon nanotube-reinforced elastomers. Vibrational Spectroscopy, **51**, 52–59 (2009). https://doi.org/10.1016/j.vibspec.2008.10.001

[74] Bokobza L., Rahmani M., Belin C., Bruneel J-L., El Bounia N-E.: Blends of carbon blacks and multiwall carbon nanotubes as reinforcing fillers for hydrocarbon rubbers. Journal of Polymer Science Part B: Polymer Physics, **46**, 1939–1951 (2008). https://doi.org/10.1002/polb.21529

[75] Medalia A. I.: Elastic modulus of vulcanizates as related to carbon black structure. Rubber Chemistry and Technology, **46**, 877–896 (1973). https://doi.org/10.5254/1.3547416

[76] Agnelli S., Pandini S., Serafini A., Musto S., Galimberti M.: Anisotropic nonlinear mechanical behavior in carbon nanotubes/poly(1,4-*cis*-isoprene) nanocomposites. Macromolecules, **49**, 8686–8696 (2016). https://doi.org/10.1021/acs.macromol.6b01682

[77] Smith W. H., Hanna N. P.: Comparison between the observed density of crystalline rubber and the density calculated from X-ray data. Rubber Chemistry and Technology, **15**, 265–271 (1942). https://doi.org/10.5254/1.3546606